Modeling nighttime ecosystem respiration from measured CO_2 concentration and air temperature profiles using inverse methods

Jehn-Yih Juang,[1] Gabriel G. Katul,[1] Mario B. S. Siqueira,[1] Paul C. Stoy,[1] Sari Palmroth,[1] Heather R. McCarthy,[1] Hyun-Seok Kim,[1] and Ram Oren[1]

[1] A major challenge for quantifying ecosystem carbon budgets from micrometeorological methods remains nighttime ecosystem respiration. An earlier study utilized a constrained source optimization (CSO) method using inverse Lagrangian dispersion theory to infer the two components of ecosystem respiration (aboveground and forest floor) from measured mean CO_2 concentration profiles within the canopy. This method required measurements of within-canopy mean velocity statistics and did not consider local thermal stratification. We propose a Eulerian version of the CSO method (CSO_E) to account for local thermal stratification within the canopy for momentum and scalars using higher-order closure principles. This method uses simultaneous mean CO_2 concentration and air temperature profiles within the canopy and velocity statistics above the canopy as inputs. The CSO_E was tested at a maturing loblolly pine plantation over a 3-year period with a mild drought (2001), a severe drought (2002), and a wet year (2003). Annual forest floor efflux modeled with CSO_E averaged 111 g C m^{-2} less than that estimated using chambers during these years (2001: 1224 versus 1328 gCm^{-2}; 2002: 1127 versus 1230 gCm^{-2}; 2003: 1473 versus 1599 gCm^{-2}). The modeled ecosystem respiration exceeded estimates from eddy covariance measurements (uncorrected for storage fluxes) by at least 25%, even at high friction velocities. Finally, we showed that the CSO_E annual nighttime respiration values agree well with independent estimates derived from the intercept of the ecosystem light-response curve from daytime eddy covariance CO_2 flux measurements.

Citation: Juang, J.-Y., G. G. Katul, M. B. S. Siqueira, P. C. Stoy, S. Palmroth, H. R. McCarthy, H.-S. Kim, and R. Oren (2006), Modeling nighttime ecosystem respiration from measured CO_2 concentration and air temperature profiles using inverse methods, *J. Geophys. Res.*, *111*, D08S05, doi:10.1029/2005JD005976.

1. Introduction

[2] Long-term measurements of net ecosystem exchange (NEE) are now routinely employed to estimate ecosystem carbon budgets using eddy covariance (EC), yet the large error in the measurement of ecosystem respiration (R_E) under nighttime conditions remains an unresolved problem that must be confronted [*Baldocchi et al.*, 1996; *Goulden et al.*, 1996; *Law et al.*, 1999a, 1999b; *Lindroth et al.*, 1998; *Moncrieff et al.*, 1996; *Schmid et al.*, 2000; *Valentini et al.*, 2000; *Wofsy et al.*, 1993]. Often, nocturnal conditions are dominated by vertical subsidence, lack of steadiness in mean atmospheric conditions, and intermittent turbulent transport often initiated by transients such as passage of clouds [*Cava et al.*, 2004]. When viewed from the one-dimensional vertically integrated scalar continuity equation, these factors contribute to increased "decoupling" between the desired R_E quantity and the CO_2 flux above the canopy, the latter being the observed quantity by EC methods.

Furthermore, these nocturnal conditions tend to amplify the limitations of the EC instrument configurations for measuring the turbulent flux. For example, separation distance between gas analyzers and anemometers, volume averaging by anemometers across some path length, and finite sampling periods that may be too short to resolve intermittency (and other low-frequency contributions) contribute to a reduction in the measured turbulent flux by EC systems [*De Bruin et al.*, 1993; *Kaimal and Finnigan*, 1994; *Kaimal and Gaynor*, 1991; *Leuning and Judd*, 1996; *Massman*, 2000; *Moncrieff et al.*, 1996].

[3] In this study, we argue that these theoretical and sampling reasons necessitate exploring other micrometeorological methods that are sensitive to different set of assumptions and approximations to constrain or independently verify nighttime R_E estimates derived from EC.

[4] An independent approach to estimating R_E is to utilize a functional relationship between aboveground mean CO_2 sources, $\overline{S}(t,z)$, or turbulent fluxes, $\overline{F}(t,z)$, and a relatively simpler quantity to measure such as mean CO_2 concentration profiles, $\overline{C}(t,z)$, within the canopy volume, where t is time, z is the height from the forest floor and the overbar denotes the temporal and spatial averaging operator. This framework is not new and dates back to *Woodwell and*

[1]Nicholas School of the Environment and Earth Sciences, Duke University, Durham, North Carolina, USA.

Dykeman [1966]. The basic premise is that $\overline{S}(t,z)$ and $\overline{F}(t,z)$ can be related to $\overline{C}(t,z)$ using the temporally and horizontally averaged one-dimensional continuity equation for a planar homogeneous flow, given by

$$\frac{\partial \overline{C}(t,z)}{\partial t} = -\frac{\partial \overline{F}(t,z)}{\partial z} + \overline{S}(t,z) \tag{1}$$

which, upon vertical integration, yields

$$\frac{\partial}{\partial t}\left[\int_0^h \overline{C}(t,z)dz\right] = -\overline{F}(t,h) + R_E \tag{2}$$

where h is the mean canopy height, and R_E is defined as

$$R_E = \int_0^h \overline{S}(t,z)dz + \overline{F}(t,0) \tag{3}$$

where $\overline{F}(t,0)$ is the forest floor efflux. In equation (2), $\overline{F}(t,z)$ (which can be measured by EC) represents R_E when $\frac{\partial}{\partial t}\left[\int_0^h \overline{C}(t,z)dz\right] = 0$. A primitive approach to compute $\overline{S}(t,z)$ in equation (1) can be formulated on the basis of $\overline{C}(t,z)$ measurement using first-order closure principles (or K-theory) by assuming that

$$\overline{F}(z) = -K_t \frac{\partial \overline{C}}{\partial z}$$

where K_t is the eddy diffusivity.

[5] Over the past 30 years, however, theoretical developments and many laboratory and field experiments have demonstrated that scalar and momentum fluxes within many canopies do not always obey K-Theory [*Corrsin*, 1974; *Deardorff*, 1972, 1978; *Denmead and Bradley*, 1985; *Finnigan*, 1985; *Raupach*, 1988; *Shaw*, 1977; *Sreenivasan et al.*, 1982; *Wilson*, 1989]. To alleviate K-Theory limitations, other theoretical and practical methods were developed without resorting to a local eddy diffusivity approximation [*Katul and Albertson*, 1999; *Raupach*, 1988, 1989a, 1989b; *Siqueira and Katul*, 2002].

[6] For example, *Lai et al.* [2002a] used the Localized Near Field (LNF) theory to relate $\overline{S}(t,z)$ to $\overline{C}(t,z)$ and demonstrated some success in estimating the two components of R_E (i.e., $\int_0^h \overline{S}(t,z)dz$ and $\overline{F}(t,0)$) over a 1-year period for near neutral and mildly stable flows. However, they pointed out a drawback of their method, titled Constrained Source Optimization (CSO), in that it was incapable of resolving the effects of local thermal stratification at a particular z within the canopy except through a Lagrangian integral timescale. Previous Lagrangian methods attempted to correct the Lagrangian timescale via a uniform multiplier derived from Monin-Obukhov similarity theory [*Hsieh et al.*, 2003; *Leuning*, 2000]. Several basic issues within Lagrangian models remain subject to debate outside the stability effects – most notable is that almost all Lagrangian models assume a vertically uniform timescale [*Lai et al.*, 2002a].

This assumption cannot be reconciled with a uniform mixing length scale inside the canopy [*Katul et al.*, 2004].

[7] On the other hand, *Siqueira et al.* [2002, 2003], and *Siqueira and Katul* [2002] developed Eulerian closure models that are capable of accounting for local thermal stratification within the canopy volume if mean air temperature profile measurements are available.

[8] This study combines the two approaches by revising the CSO method of *Lai et al.* [2002a] to include local thermal stratification within the canopy volume using higher-order closure principles. We tested this modified CSO method over a 3-year period at a maturing southeastern pine forest using independent measurements of $\int_0^h \overline{S}(t,z)dz$ and $\overline{F}(t,0)$. The study period includes a mild drought (2001), a severe drought (2002), and a very wet year (2003) so that widest ranges of hydrologic and climatic conditions at this site are sampled. Improvements over R_E estimation from EC measurements using standard friction velocity $u*$ thresholds are discussed within the context of annual carbon balances.

2. Theory

2.1. Governing Equations and Turbulent Transport

[9] Rather than using K-theory, we consider the steady state one-dimensional budget equation for the temporally and horizontally averaged carbon flux for high Reynolds and Peclet numbers flows (i.e., the molecular diffusion and conductive heat transfer are neglected), given by:

$$\frac{\partial \overline{F}}{\partial t} = 0 = -\overline{w'w'}\frac{\partial \overline{C}}{\partial z} + \frac{g}{\overline{T}}\overline{T'C'} - \overline{C'\frac{\partial p'}{\partial z}} - 2\varepsilon_C - \frac{\partial \overline{w'w'C'}}{\partial z} \tag{4}$$

where w is the vertical velocity, $\overline{T}$ is the mean air temperature, p is the turbulent static pressure normalized by air density ρ, g is the gravitational acceleration constant, and ε_C is the molecular dissipation term. The symbol prime denotes the departures from averaging operator. To solve equation (4) from measured mean CO_2 concentration profiles, further parameterizations are needed to quantify the vertical velocity variance $\overline{w'w'}$, the covariance between temperature and CO_2 turbulent fluctuations $\overline{T'C'}$ (i.e., the local atmospheric stability effects), the concentration-pressure interaction term $\overline{C'\frac{\partial p'}{\partial z}}$, the flux dissipation term ε_C, and the triple moment $\overline{w'w'C'}$. For $\overline{w'w'}$, we employ a second-order closure model [*Katul and Albertson*, 1998; *Wilson and Shaw*, 1977] that solves for the mean velocity $\overline{u_i}$ and Reynolds stresses $\overline{u_i'u_j'}$, as discussed in Appendix A.

[10] In equation (4), the air temperature $\overline{T}$ and $\overline{T'C'}$ need to be determined. The corresponding steady state one-dimensional temporal and horizontally averaged budget equations of the mean air temperature $\overline{T}(t,z)$ and the vertical kinematic turbulent flux of sensible heat $\overline{F_T}(t,z)$ can be derived as:

$$\frac{\partial \overline{T}(t,z)}{\partial t} = 0 = -\frac{\partial \overline{F_T}(t,z)}{\partial z} + \overline{S_T}(t,z) \tag{5}$$

$$\frac{\partial \overline{F_T}}{\partial t} = 0 = -\overline{w'w'}\frac{\partial \overline{T}}{\partial z} + \frac{g}{\overline{T}}\overline{T'T'} - \overline{T'\frac{\partial p'}{\partial z}} - 2\varepsilon_T - \frac{\partial \overline{w'w'T'}}{\partial z} \tag{6}$$

where ε_T is the molecular dissipation term for sensible heat, and $\overline{S_T}(t,z)$ is the corresponding heat source/sink term at level z.

[11] Unlike the LNF approach utilized by *Lai et al.* [2002a], the covariance $\overline{T'C'}$ and variance $\overline{T'T'}$ explicitly characterize the local (i.e., at given level z within the canopy) buoyant production/destruction effects. To compute the budgets of these two variables, additional steady state one-dimensional prognostic equations are needed and given by *Meyers and Paw U* [1987]:

$$\frac{\partial \overline{T'C'}}{\partial t} = 0 = -\overline{F_T}\frac{\partial \overline{C}}{\partial z} - \overline{F}\frac{\partial \overline{T}}{\partial z} - 2\varepsilon_{TC} - \frac{\partial \overline{w'T'C'}}{\partial z} \qquad (7)$$

and

$$\frac{\partial \overline{T'T'}}{\partial t} = 0 = -2\overline{F_T}\frac{\partial \overline{T}}{\partial z} - 2\varepsilon_{TT} - \frac{\partial \overline{w'T'T'}}{\partial z} \qquad (8)$$

where ε_{TC} and ε_{TT} are the corresponding molecular dissipation terms.

[12] In equations (4), (6), (7), and (8), the pressure-gradient diffusion terms $T'\frac{\partial p'}{\partial z}$, $C'\frac{\partial p'}{\partial z}$, molecular dissipation terms ε_T, ε_C, ε_{TC}, ε_{TT}, and triple correlation terms $\overline{w'w'C'}$, $\overline{w'w'T'}$, $\overline{w'T'T'}$, $\overline{w'T'C'}$ are unknowns that need parameterizations. To solve these additional variables, standard second-order closure approximations are employed [*Donaldson*, 1973; *Katul and Albertson*, 1998; *Mellor*, 1973; *Mellor and Yamada*, 1974; *Meyers and Paw U*, 1986, 1987; *Wilson and Shaw*, 1977]. After utilizing these closure parameterizations, equations (4), (6), (7), and (8) can be rewritten as

$$\frac{\partial \overline{F}}{\partial t} = 0 = -\overline{w'w'}\frac{\partial \overline{C}}{\partial z} + \frac{g}{\overline{T}}\overline{T'C'} - \frac{Q}{3\lambda_2}\overline{F} - 2\frac{Q}{\lambda_3}\overline{F}$$
$$- \frac{\partial}{\partial z}\left[-2Q\lambda_1\frac{\partial \overline{F}}{\partial z}\right] \qquad (9)$$

$$\frac{\partial \overline{F_T}}{\partial t} = 0 = -\overline{w'w'}\frac{\partial \overline{T}}{\partial z} + \frac{g}{\overline{T}}\overline{T'T'} - \frac{Q}{3\lambda_2}\overline{F_T} - 2\frac{Q}{\lambda_3}\overline{F_T}$$
$$- \frac{\partial}{\partial z}\left[-2Q\lambda_1\frac{\partial \overline{F_T}}{\partial z}\right] \qquad (10)$$

$$\frac{\partial \overline{T'C'}}{\partial t} = 0 = -\overline{F_T}\frac{\partial \overline{C}}{\partial z} - \overline{F}\frac{\partial \overline{T}}{\partial z} - 2\frac{Q}{\lambda_3}\overline{T'C'} - \frac{\partial}{\partial z}\left[-Q\lambda_1\frac{\partial \overline{T'C'}}{\partial z}\right] \qquad (11)$$

and

$$\frac{\partial \overline{T'T'}}{\partial t} = 0 = -2\overline{F_T}\frac{\partial \overline{T}}{\partial z} - 2\frac{Q}{\lambda_3}\overline{T'T'} - \frac{\partial}{\partial z}\left[-Q\lambda_1\frac{\partial \overline{T'T'}}{\partial z}\right] \qquad (12)$$

where Q is the characteristic turbulent velocity (square root of the mean turbulent kinetic energy $\sqrt{\overline{u_i'u_i'}}$); λ_1, λ_2, λ_3 are length scales for the various terms as in *Wilson and Shaw* [1977] and *Katul and Albertson* [1998], and

physically represent the characteristic length scales for the triple velocity correlations, the pressure-velocity gradient correlations, and the viscous dissipations, respectively. The parameterizations for these length scales are discussed in Appendix A.

[13] Coupling equations (1), (5), (9), (10), (11), and (12) with the set of equations (A1) for momentum in Appendix A (mainly to solve for Q and $\overline{w'w'}$) results in 6 equations with 8 unknowns ($\overline{T}$, $\overline{C}$, $\overline{S}$, $\overline{S_T}$, $\overline{F}$, $\overline{F_T}$, $\overline{T'C'}$, $\overline{T'T'}$). If $\overline{C}(t,z)$ and $\overline{T}(t,z)$ measurements are available, the system reduces to 6 equations with 6 unknowns thereby permitting one to numerically determine $\overline{S}(t,z)$, $\overline{F}(t,z)$ and, in turn, R_E.

2.2. Eulerian Inverse Model for Heat

[14] We used the Eulerian inverse model proposed by *Siqueira and Katul* [2002] to determine $\overline{S_T}(t,z)$ and $\overline{F_T}(t,z)$ from mean air temperature profile measurement. These variables are needed to solve equations (5), (10), and (12). The boundary conditions for $\overline{F_T}(t,z)$ and $\overline{T'T'}$ are as proposed by *Meyers and Paw U* [1987] and are applied to equations (10) and (12), respectively. After estimating $\overline{F_T}(t,z)$ and $\overline{T'T'}$ from measured temperature profiles, the heat source term $\overline{S_T}(t,z)$ can be directly determined from equation (5).

[15] The advantage of this inverse model is that the effects of atmospheric stability within the canopy volume can be explicitly considered. As discussed by *Siqueira and Katul* [2002], the impact of atmospheric stability is most pronounced in the scalar-temperature covariance equations ($\overline{T'C'}$ and $\overline{T'T'}$). These terms are now directly considered via their budget equations.

2.3. Source Calculation

[16] We estimate the CO_2 turbulent fluxes and source terms differently from temperature for several reasons: (1) The aboveground plant area density is indicative of the relative "distribution" of aboveground respiring biomass thereby providing an additional constraint on $\overline{S}(t,z)$; (2) small errors in measured mean CO_2 concentration profile can dramatically impact the inference of $\overline{S}(t,z)$ from measured $\overline{C}(t,z)$ because of the absence of any redundancy [*Siqueira et al.*, 2003]; and (3) the temperature sensitivity of $\overline{S}(t,z)$, while not precisely known, can be constrained from leaf measurements.

[17] The estimation of $\overline{S}(t,z)$ at each level from measured $C(t,z)$ can be reformulated as an optimization problem [*Lai et al.*, 2002a; *Styles et al.*, 2002] in which the relative strength of $\overline{S}(t,z)$ and its temperature sensitivity is a priori defined. Thus, rather than solving equations (1), (5), (9), (10), (11), and (12) for $\overline{S}(t,z)$ forced by mean CO_2 concentration profile measurements, the system can be forced by an estimate of $\overline{S}(t,z)$ and predict the mean CO_2 concentration distribution, which can in turn be compared to measurements (e.g., every half hour).

[18] To formulate a model for $\overline{S}(t,z)$, we note that the woody and leaf foliage tissue respiration have different physiological properties and hence their contribution to the total aboveground respiration is different. However, *Lai et al.* [2002a] argued that in a first-order analysis, the respiration of woody tissue is less important than the contribution from foliage because the total woody surface area is less than the total leaf surface area (at least for

this pine site), and the woody parts have smaller tissue-specific respiration rates than the foliage [*Hamilton et al.*, 2002]. With this simplification, *Lai et al.* [2002a] estimated the carbon source vertical distribution $\overline{S}(t,z)$ by assuming that the entire plant surface area was only foliage leading to:

$$\overline{S}(t,z) = a(t,z) \cdot R_d(t,z) \tag{13}$$

where $a(t,z)$ is the plant area density (PAD, in $m^2\ m^{-3}$), and $R_d(t,z)$ is the dark respiration rate per unit plant tissue surface area (in $\mu mol\ m^{-2}\ s^{-1}$). $R_d(t,z)$ can be estimated from the *Farquhar et al.* [1980] model:

$$R_d(t,z) = \alpha(t) \cdot V_{c\max}(t,z) \tag{14}$$

where $\alpha(t)$ is a constant that needs to be determined at a given time t, and $V_{c\max}(t,z)$ is the maximum catalytic capacity of Rubisco per unit leaf area. The temperature dependency of $V_{c\max}(t,z)$ can be expressed as:

$$V_{c\max}(t,z) = V_{c\max,25}(t,z) \cdot \frac{\exp\left[a_1\left(\overline{T}(t,z) - 25\right)\right]}{1 + \exp\left[a_2\left(\overline{T}(t,z) - 41\right)\right]} \tag{15}$$

where a_1 and a_2 are the species-specific adjustment coefficients, which are obtained experimentally (e.g., via porometry) and $V_{c\max,25}(t,z)$ is the value of $V_{c\max,25}(t,z)$ at $25°C$ [*Campbell and Norman*, 1998; *Collatz et al.*, 1991; *Farquhar et al.*, 1980]. From previous studies conducted at the site [*Ellsworth*, 1999; *Naumburg and Ellsworth*, 2000; *Naumburg et al.*, 2001], $V_{c\max,25}$, a_1 and a_2 are 59 $\mu mol\ m^{-2}\ s^{-1}$, 0.051 and 0.205, respectively for the upper canopy pine foliage, and are 30 $\mu mol\ m^{-2}\ s^{-1}$, 0.088 and 0.290, respectively for the subcanopy broadleaved plants [*Lai et al.*, 2002a]. With the exception of the product $\{\alpha(t) \cdot V_{c\max,25}(t,z)\}$ these physiological parameters were considered temporally constant for the model calculations.

2.4. Modified Constrained Source Optimization

[19] With this formulation for $\overline{S}(t,z)$, the problem reduces to a two-parameter estimation ($\{\alpha(t) \cdot V_{c\max,25}(t,z)\}$ and $\overline{F}(t,0)$) from the measured nighttime CO_2 concentration profiles $\overline{C}(t,z)$. Thus the question is what is the optimum combination of $\{\alpha(t) \cdot V_{c\max,25}(t,z)\}$ and $\overline{F}(t,0)$ so that that the solution to equations (1), (5), (9), (10), (11), and (12) best matches the measured $\overline{C}(t,z)$? Because only two parameters describe the entire source and they can be constrained to vary within a limited range, a global search for the optimum $\{\alpha(t) \cdot V_{c\max,25}(t,z)\}$ and $\overline{F}(t,0)$ can be conducted until the root mean square error (RMSE) between the calculated and measured CO_2 concentrations at different levels is minimized on a 30-min timescale. For example, if foliage respiration is the only dominant above-ground respiration component, we anticipate $\alpha(t)$ to be near 0.015, which is a commonly used value in many studies [*Collatz et al.*, 1991; *Farquhar et al.*, 1980; *Lai et al.*, 2002a]. Furthermore, nighttime forest floor respiration should not exceed the maximum daytime photosynthesis in magnitude. An upper limit on the maximum daytime canopy photosynthesis $A_{n,c}$ can be determined from day-time water vapor flux measurements (i.e., latent heat flux) using

$$A_{n,c} \approx \frac{LE}{VPD}\left(1 - \frac{C_i}{C_a}\right)C_a$$

where *LE* is determined as the maximum latent heat flux measured for each day throughout the experiment, *VPD* is the mean daytime vapor pressure deficit and C_i/C_a is the ratio of intercellular to ambient atmospheric CO_2 concentration, estimated at 0.66 for sunlit foliage [*Katul et al.*, 2000]. This leads to a maximum conservative estimate of mean photosynthesis and sets an upper limit to a priori constrain nighttime respiration. Because of these constraints and its Eulerian formulation to account for thermal stratification within the canopy, we refer to this method as the Eulerian constrained source optimization (CSO_E).

3. Study Site and Measurements

3.1. Study Site

[20] The measurements were made at the Blackwood Division of the Duke Forest near Durham in North Carolina (site location: 35°58′N, 79°05′W, 163 m above sea level) as part of the AmeriFlux long-term CO_2 flux monitoring initiative [*Baldocchi et al.*, 2001]. This study site is a uniformly planted loblolly pine (*Pinus taeda L.*) forest (planted in 1983 at 2 m × 2.4 m spacing) that extends 300 to 600 m in the east-west direction and 1000 m in the south-north direction. The subcanopy also contains about 40 woody species, of which *Liquidambar styraciflua L.*, *Acer rubrum L.*, *Ulmus alata Michx.*, and *Cornus florida L.* are the most prevalent [*Palmroth et al.*, 2005]. The local topographic variations are small (slope < 5%) enough to ignore the effect of the complex terrain on the flow statistics [*Siqueira et al.*, 2002]. The study period extends from year 2001 to 2003. Table 1 describes the variations in ecological, hydrologic, and climatic conditions for these 3 years at this study site.

3.2. Eddy Covariance Flux Measurements

[21] The momentum components, Reynolds stresses, sensible heat, latent heat and CO_2 fluxes above the canopy were measured by a conventional eddy covariance system comprising a Li-Cor 7500 CO_2/H_2O open-path infrared gas analyzer (Li-Cor Inc., Lincoln, Nebraska, USA) and a triaxial sonic anemometer (CSAT3, Campbell Scientific Inc., Logan, Utah, USA). Both the gas analyzer and the triaxial sonic anemometer were positioned at $z = 20.23$ m, which is above the canopy top (from 17 to 18 m during the study period).

[22] The flux measurements were sampled using a Campbell Scientific 23X data micrologger with all digitized signals transferred to a portable computer via an optically isolated RS232 interface for future processing. All the variables in this eddy covariance measuring system were sampled at 10 Hz and averaged every 30 min. The correction for the effects of air density on flux measurements after *Webb et al.* [1980] was applied.

3.3. Mean CO_2 Concentration and Air Temperature Profiles Within the Canopy

[23] A multilayer concentration monitoring system was installed to sample the mean water vapor pressure and CO_2

Table 1. Overall Variability Ranges in Ecophysiological, Hydrological, and Climatic Factors From 2001 to 2003 at the Duke Forest Pine Site[a]

Year	2001	2002	2003
Average canopy height, m	17.0	17.5	18.0
Total PAI range, $m^2 m^{-2}$	$2.20 \sim 6.53$	$2.22 \sim 5.16$	$2.09 \sim 4.16$[b]
Pine PAI range, $m^2 m^{-2}$	$1.85 \sim 3.26$	$1.91 \sim 2.96$	$1.74 \sim 3.23$[b]
Growing season[c] precipitation, mm	529.2	371.4	789.8
Soil moisture content (θ) range, $m^3 m^{-3}$	$0.13 \sim 0.54 \ (0.13 \sim 0.51)$[d]	$0.13 \sim 0.47 \ (0.13 \sim 0.37)$	$0.20 \sim 0.54 \ (0.20 \sim 0.54)$
Soil temperature (T_s) range, °C	$3.1 \sim 23.5 \ (8.8 \sim 23.5)$	$5.4 \sim 23.8 \ (9.6 \sim 23.8)$	$3.7 \sim 23.6 \ (9.0 \sim 23.6)$
Air temperature (T_a) range, °C	$-11.2 \sim 35.5 \ (-2.8 \sim 35.5)$	$-10.7 \sim 38.9 \ (-2.6 \sim 38.9)$	$-12.2 \sim 35.2 \ (0.3 \sim 35.2)$

[a]The soil moisture content, soil temperature, and the air temperature are half-hourly averages from the profile measurement.
[b]In December of 2002, an ice storm reduced the PAI of the pine stand.
[c]The growing season is from 1 April to 30 September (Julian day: 152 to 273).
[d]The bracketed numbers represents the range during the growing season.

concentration at 10 different levels throughout the canopy volume ($z = 0.1$ m, 0.75 m, 1.5 m, 3.5 m, 5.5 m, 7.5 m, 9.5 m, 11.5 m, 13.5 m and 15.5 m) using a Li-Cor 6262 CO_2/H_2O infrared gas analyzer. This profiling system includes a multi-port gas-sampling manifold to sample each level for 1 min (45 s sampling and 15 s purging) with a repeating cycle of 10 min for the 10 sampled levels. Data were averaged every 30 min. In addition, a mean air temperature profiling system was installed to measure the mean air temperature every 30 min at eight different levels ($z = 1.5$ m, 3.5 m, 5.5 m, 7.5 m, 9.5 m, 11.5 m, 13.5 m, and 15.5 m) throughout the canopy volume using copper-constantan shielded thermocouple sensors (see *Siqueira and Katul* [2002] for details).

3.4. Volumetric Soil Moisture Content and Soil Temperature Measurement

[24] Long-term volumetric soil moisture content θ ($m^3 m^{-3}$) was sampled using 4 Campbell Scientific CS615 reflectometers placed in the top 30 cm of the mineral soil, and the soil temperature was measured at $10-12$ cm via nonlinear thermistor probes (M 841/S1, Siemens, Germany). All signals were sampled every 30 s using a CR23X data logger and averaged every 30 min. The mean soil moisture content was obtained by averaging over all 4 CS615 probes.

3.5. Forest Floor CO_2 Efflux Measurements

[25] The forest floor CO_2 efflux was measured with the automated carbon efflux system (ACES, US Patent 6692970) developed by the USDA Forest Service, Southern Research Station Laboratory in Research Triangle Park, North Carolina [*Butnor and Johnsen*, 2004; *Butnor et al.*, 2003; *Palmroth et al.*, 2005]. The ACES is an open system with an infrared gas analyzer connected to several soil chambers equipped with soil and air thermocouples, pressure equilibration ports, and reflective covers. The ACES system was installed at the site in February of 2001. The details of the ACES configuration, quality checks, and spatial sampling area, are described by *Palmroth et al.* [2005].

[26] To quantify the variation of forest floor efflux with varying volumetric soil moisture content θ ($m^3 m^{-3}$) and soil temperature T_s (°C), *Palmroth et al.* [2005] derived a equation modified from *Fang and Moncrieff* [1999], of the form

$$F(t, 0) = R_b e^{aT_s} \lfloor 1 - e^{(-b\theta+c)} \rfloor \qquad (16)$$

where R_b is the base respiration ($\mu mol \ m^{-2} \ s^{-1}$), which is defined as the intercept at 0°C, a is the temperature

sensitivity ($Q_{10} = e^{a \times 10}$) when soil moisture content is not limiting, and the constants b and c are fitted parameters of the soil moisture reduction function. All the constants in equation (16) were determined via nonlinear regression methods using the ACES measured respiration, the mean $10-12$ cm soil temperature, and the CS615 soil moisture and are summarized in Table 2 [*Palmroth et al.*, 2005]. Equation (16) constitutes the spatially averaged chamber measurements of forest floor efflux and will be used to independently test the CSO_E estimates of $\overline{F}(t, 0)$.

3.6. Plant Area Index and Plant Area Density

[27] The plant area index (PAI, $m^2 \ m^{-2}$) is routinely measured several times a year using a pair of Li-Cor LAI 2000 optical sensors. The plant area density (PAD, $m^2 \ m^{-3}$) measurements were conducted at 1 m intervals from the bottom to the top of canopy. Calibration of PAI was done using allometric relationships derived from different individual species within the canopy volume [*Lai et al.*, 2000b; *Pataki et al.*, 1998; *Schafer et al.*, 2003].

[28] LAI-2000 measurements, coupled with the above-mentioned allometric functions, were used to estimate the vertical distribution of PAD at daily time steps [*Schafer et al.*, 2003]. The range of total PAI and pine PAI in 2001, 2002, and 2003 are given in Table 1.

4. Results and Discussion

[29] To address the study objective, the results and discussion are organized as follows: (1) We use the

Table 2. Regression Parameters for the Chamber-Based Forest Floor CO_2 Efflux Equation $F(t, 0) = R_b e^{aT_s} \lfloor 1 - e^{(-b\theta+c)} \rfloor$ Given by *Palmroth et al.* [2005] for 2001 to 2003 at the Duke Forest Site[a]

Day	R_b	A	b	c
		2001		
$001 \sim 179$	0.570	0.123	25.228	2.301
$180 \sim 365$	0.648	0.118	27.120	2.882
		2002		
$001 \sim 088$	0.648	0.118	27.120	2.882
$089 \sim 238$	0.908	0.092	27.952	3.099
$239 \sim 365$	0.753	0.106	32.302	3.987
		2003		
$001 \sim 365$	0.814	0.104	32.302	3.987

[a]The 2003 data are added to the data published by *Palmroth et al.* [2005], which covered $2001-2002$.
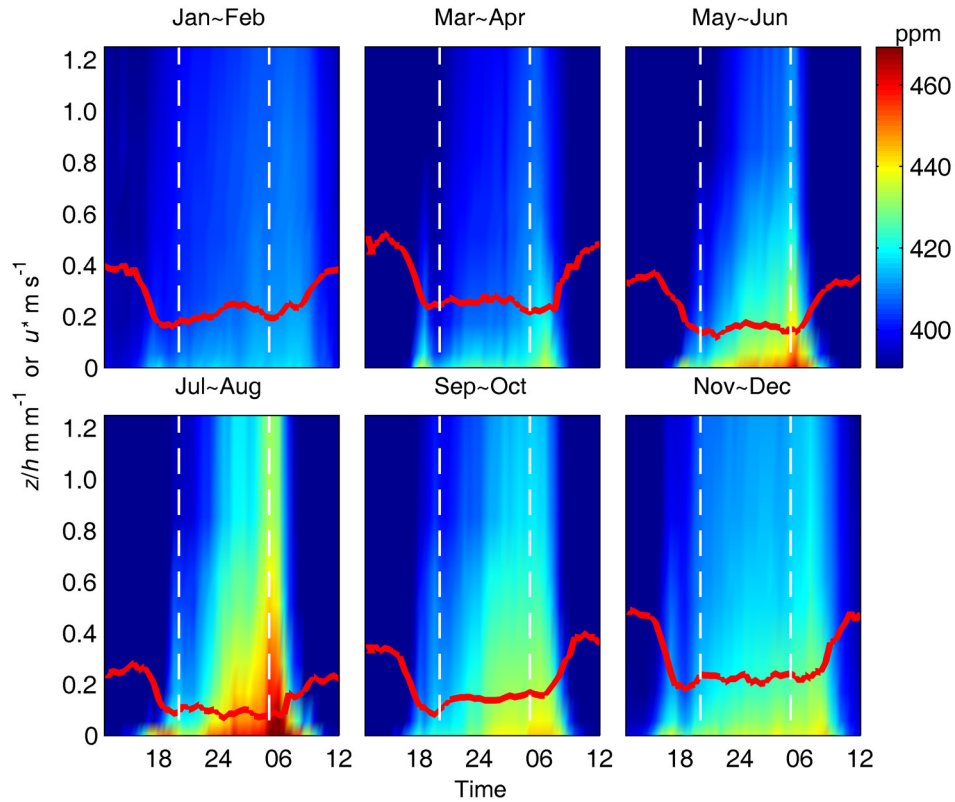
Figure 1. Normalized depth/time of day variations of nighttime (2000 to 0500 LT, bounded by two dashed lines in each subplot) ensemble averaged CO_2 concentration profiles (ppm) for 2-month periods in 2003. The 2-month ensemble averaged friction velocity $u*$ (m s^{-1}, solid red line) is shown for reference.

measured $\overline{C}(t,z)$ to estimate the nighttime storage fluxes in equation (1) and compare their magnitude to the EC measured nighttime NEE noting that almost all sites that utilize a large $u*$ threshold for the EC data neglect storage fluxes in equation (1). (2) We use the CSO$_E$ model to individually estimate the two components of nighttime ecosystem respiration and compare them to the results from chamber measurements and to independent estimates of aboveground respiration. (3) We discuss the sensitivity of the modeled R_E to local thermal stratification by comparing model calculations with and without the consideration of buoyant production/destruction terms for thermally stratified condition and neutral flows condition, respectively. (4) Finally, we discuss the CSO$_E$ respiration components within the context of the annual carbon balance at the site, and explore other methods to constrain annual nighttime ecosystem respiration (e.g., intercept of the NEE light response curve).

[30] To ensure that nighttime conditions are not "contaminated" by photosynthesis, we define nighttime hereafter from 2000 to 0500 LT throughout the 3-year study period.

4.1. Storage Flux

[31] Gap-filled nighttime EC measured flux (hereafter referred to as $\overline{F_{EC}}$) is often derived from high $u*$ runs, in which the canopy is likely to be ventilated (except for a region close to the ground).

Under such conditions, it is reasonable to assume that $\overline{F_{st}} = \left| \dfrac{\partial}{\partial t} \left[\displaystyle\int_0^h \overline{C}(t,z)dz \right] \right| \ll |\overline{F_{EC}}|$. Hence, when determining time series of R_E, $\overline{F_{st}}$ is often neglected when using gap-filled $\overline{F_{EC}}$ collected for high $u*$. On a daily basis, the mean value of $\overline{F_{st}}$ is often close to zero, but can be significantly large during sunrise, sunset and during nighttime conditions of low $u*$ [Lai et al., 2000a, 2002a].

[32] Because $\overline{C}(t,z)$ is the key determinant of $\overline{F_{st}}$, we show the 2-month ensemble averaged $\overline{C}(t,z)$ (in ppm) measured at different times of the day during 2003 for illustration (Figure 1). It is clear that the mean CO_2 concentration is unsteady during nighttime conditions and this buildup trend is even stronger during high leaf area season (i.e., May to October). This finding is not surprising because the canopy respires more during the summer months, because of both higher leaf mass and higher temperature, and because the turbulence is dampened during the high leaf area season (see Appendix A). More subtle is the observation that the temporal variation of the measured ensemble averaged $u*$ (red solid line) is also different across seasons with lower values measured in the summer. This finding is important when using a global $u*$ threshold for gap filling $\overline{F_{EC}}$ measurements because such a threshold may disproportionately eliminate summertime runs.

[33] To quantify the effect of nighttime variations in $u*$ on EC and storage flux, we compared $\overline{F_{st}}/\overline{F_{EC}}$ at different
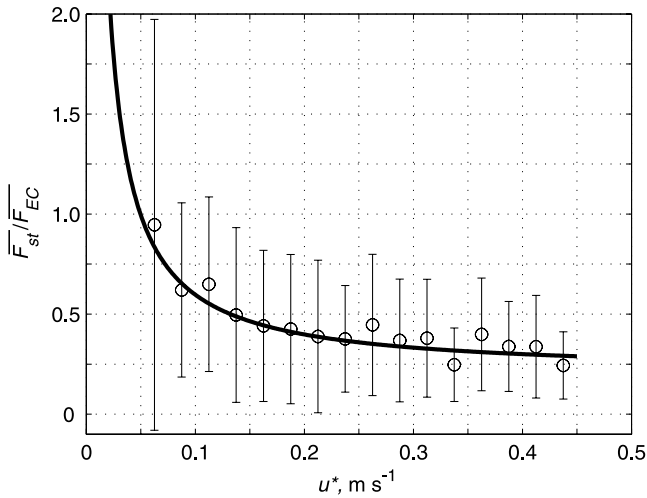
Figure 2. Ensemble variation of the ratio of storage flux to EC measured flux ($\overline{F_{st}}/\overline{F_{EC}}$) with friction velocity u^* during nighttime runs (2000 to 0500 LT) for the entire measurement period (2001–2003). The flux ratio $\overline{F_{st}}/\overline{F_{EC}}$ is expressed as 14-day ensemble averages, and vertical bars represent one standard deviation. The solid line is the regression curve.

u^* thresholds (Figure 2, showing 14-day averages during nighttime from the entire 3-year study period). The value of $\overline{F_{st}}$ is derived from the numerical integration of the mea-sured mean CO_2 concentration profile every 30 min run and ensemble averaged every 14 days.

[34] Figure 2 indicates that the ensemble averaged $\overline{F_{st}}/\overline{F_{EC}}$ is almost always greater than 0.27 at this experimental site. The mean $\overline{F_{st}}/\overline{F_{EC}}$ ratio increases from 0.27 to about 0.44 when u^* drops from 0.45 to 0.15 m s^{-1}, but significantly increases when u^* drops below 0.15 m s^{-1}. Note also that measured $u^* < 0.15$ m s^{-1} is a common occurrence for summertime runs, especially in 2003 (Figure 1). Thus this analysis indicates that R_E may be larger than $\overline{F_{EC}}$ by at least 27% at this experimental site if storage is neglected. However, we emphasize that determining $\overline{F_{st}}$ from a single tower is subject to several theoretical and practical limitations, and the need to ensemble average concentration data (e.g., 14-day) beyond averaging random noise are further discussed in Appendix B.

4.2. Optimized Forest Floor Carbon Efflux

[35] The optimized $\{\alpha(t) \cdot V_{cmax,25}(t, z)\}$ and $\overline{F}(t, 0)$ were determined over a 14-day ensemble average period on the basis of the root mean squared error ($RMSE \leq 10$ ppm) of 30-min comparisons between CSO$_E$ modeled and measured $\overline{C}(t, z)$. The available numbers of 30-min runs used in the model calculations for 2001 to 2003 are 396, 432, and 450 runs, respectively. The resulting CSO$_E$ optimized $\overline{F}(t, 0)$ is then regressed with measured 10–12 cm soil temperature T_s (Figure 3a). The relationship is expressed as

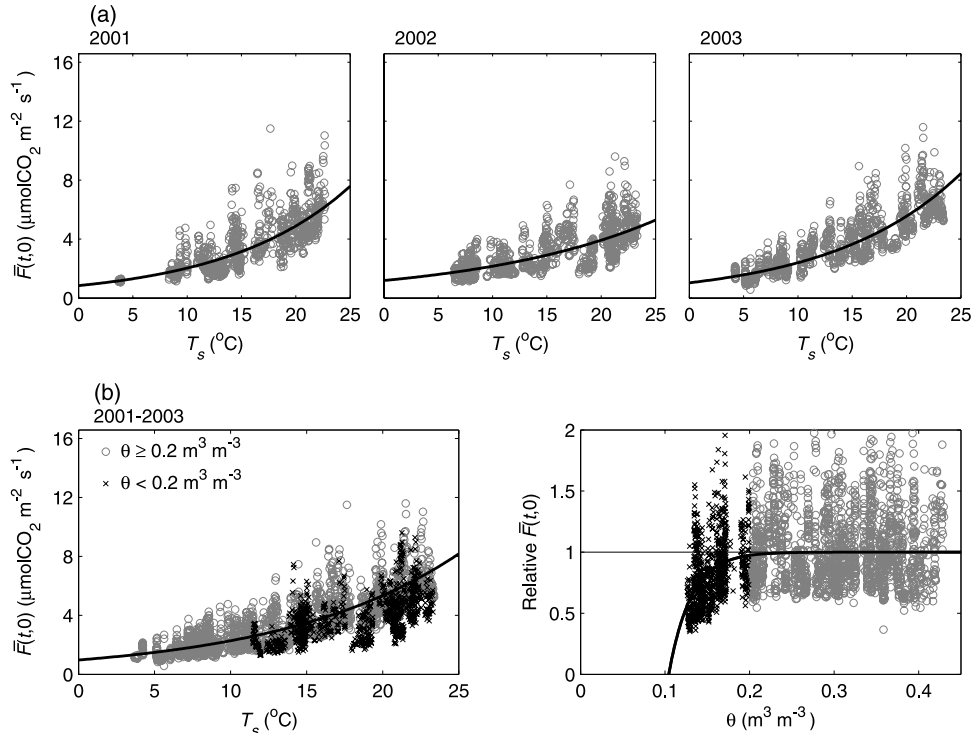$$F(t, 0) = A \cdot \exp(B \cdot T_s(t)) \tag{17}$$

Figure 3. (a) Variation of the CSO$_E$ optimized forest floor efflux (open circle) with soil temperature for each of the 3 years. The solid lines are obtained by regressing soil temperature to the CSO$_E$ optimized values of $\overline{F}(t, 0)$. They demonstrate the nonstationarity in forest floor respiration-soil temperature curve parameters. (b) Soil temperature effect (left plot) for $\theta \geq 0.2$ m^3 m^{-3} and soil moisture reduction curve (solid line on the right plot) for all 3 years. All equations and regression statistics are shown in Table 3.

Table 3. Regression Curves for $F(t, 0)$ Shown in Figure 3[a]

Year	Fitted Curve	R^2	RMSE	Q_{10}
	Ts-Dependent Only			
2001	$F(t, 0) = 0.846 \cdot \exp(0.085 \cdot T_s)$	0.66	1.08	2.34
2002	$F(t, 0) = 1.191 \cdot \exp(0.060 \cdot T_s)$	0.55	1.22	1.82
2003	$F(t, 0) = 1.036 \cdot \exp(0.084 \cdot T_s)$	0.76	1.03	2.32
	Unique Fitted Curve Couple With θ Correction			
2001−2003	$F(t, 0) = F_{Ts} \cdot [1 - \exp(-37.829\theta + 3.948)]$	0.52	1.12	2.09
T_s dependence	$F_{Ts} = 0.974 \cdot \exp(0.085 \cdot T_s)$	0.73	1.05	2.34
θ correction	$1 - \exp(-37.829\theta + 3.948)$	0.15	N/A	N/A

[a]Unit is μmol m^{-2} s^{-1}. The coefficient of determination R^2 and the root mean squared error RMSE (in μmol m^{-2} s^{-1}) are also shown. For reference, we also show the equivalent Q_{10} values.

where A and B are regression parameters (Figure 3a; with an individual regression fit for each year) presented in Table 3. From Table 3, it is clear that these fitted parameters change from year to year. For example, forest floor carbon efflux values modeled with CSO$_E$ for the severe drought year of 2002 were different than the other 2 years, especially when soil temperature was high (Figure 3a). Calculated from parameter B, the Q$_{10}$ values for 2001, 2002 and 2003 are 2.34, 1.82 and 2.32, respectively, consistent with the values reported by *Palmroth et al.* [2005]. Using a Student's t-test, the reduction in Q$_{10}$ for 2002 is statistically significant at the 95% confidence level.

[36] To investigate whether the variability in parameters are driven by soil moisture effects, we fit equation (16) [*Palmroth et al.*, 2005] to the entire 3-year record. We separate the model results into two different θ regions ($\theta \geq$ 0.2 m^3 m^{-3} and $\theta <$ 0.2 m^3 m^{-3}), where the value of $\theta <$ 0.2 m^3 m^{-3} is the critical point at which θ significantly affects $\overline{F}(t, 0)$ [*Palmroth et al.*, 2005]. For the non-soil-moisture-limiting region, it is clear from Figure 3b that one temperature curve suffices to explain the entire optimized forest floor flux variability (hereafter, the estimate of $\overline{F}(t, 0)$ from this curve is referred to as F_{Ts}). For the soil-moisture-limiting region, we plot relative $\overline{F}(t, 0)$ (expressed as $\overline{F}(t, 0)/F_{Ts}$) against θ and show that resulting reduction is

consistent with the chamber data. When combining these two findings, a unique multivariate curve for the entire 3-year record can be derived (Table 3).

4.3. Optimized Aboveground C Source

[37] There are no explicit measurements for the aboveground respiration during this period and hence the evaluation of the CSO$_E$ model is not direct. Nonetheless, we can assess whether the CSO$_E$ model is sensitive to well-documented variability in $V_{cmax,25}(t, z)$. Toward this end, we compare the seasonal dynamics in $\{0.015 \cdot V_{cmax,25}(t, z)\}$ as derived from porometry [*Ellsworth*, 2000] with the optimized $\{\alpha \cdot V_{cmax,25}(t, z)\}$ from the CSO$_E$.

[38] If we set $\alpha = 0.015$ and compute $V_{cmax,25}(t, z)$ via equations (14) and (15), the normalized seasonal variation of $V_{cmax,25}$ (expressed as $V_{cmax,25}$/mean $V_{cmax,25}$) derived from the CSO$_E$ model calculations can be compared to the porometry data shown in Figure 4. The comparison with the porometry data cannot be direct because the published porometry measurements given by *Ellsworth* [2000] were conducted from 1998 to 2000. Nonetheless, the qualitative agreement in Figure 4 suggests that the mean CO$_2$ concentration profile data, when combined with the CSO$_E$ model, can resolve seasonal shifts in aboveground physiological properties due to leaf acclimation. This agreement
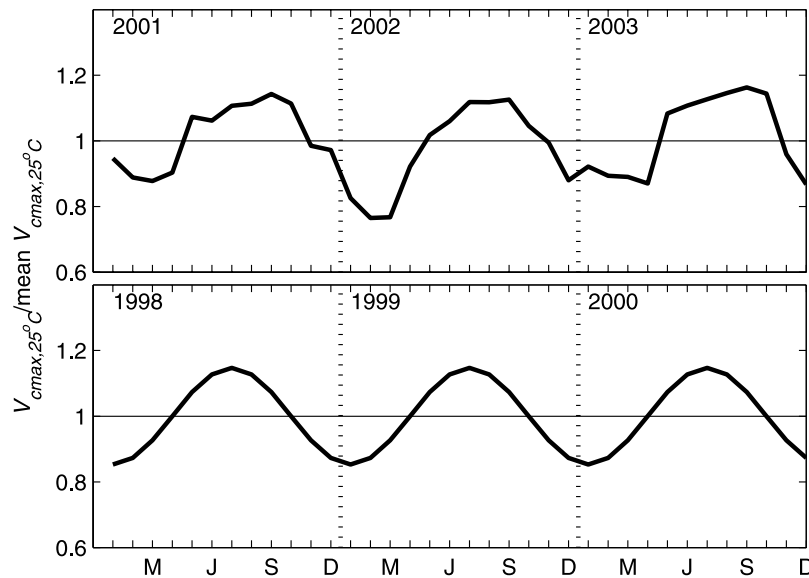

Figure 4. (top) Relative variation of optimized $V_{cmax,25}$ from CSO$_E$ model from 2001 to 2003 and (bottom) the reported relative changes in $V_{cmax,25}$ from 1998 to 2000 after *Ellsworth* [2000].
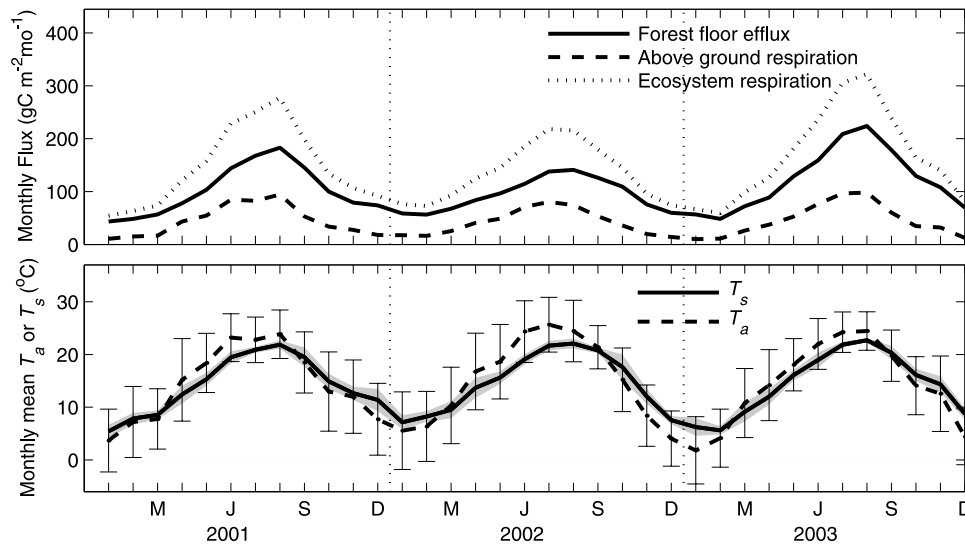
Figure 5. (top) CSO_E model results for monthly forest floor efflux, aboveground respiration, and ecosystem respiration and (bottom) monthly mean air temperature and soil temperature from 2001 to 2003. The error bars and shaded area in Figure 5 (bottom) represent the standard deviation of air temperature and soil temperature, respectively.

also lends indirect support to the CSO_E above ground respiration estimates.

4.4. Ecosystem Respiration

[39] From the optimized $\{\alpha \cdot V_{cmax,25}(t, z)\}$ and $\overline{F}(t, 0)$ described in the previous two sections, we proceed to estimate the ecosystem respiration. Figure 5 shows separately the modeled monthly variation of $\overline{F}(t, 0)$, aboveground respiration, and R_E (in gC m^{-2} month^{-1}) from 2001 to 2003, along with measured monthly averaged air and soil temperature. On the basis of the CSO_E calculations, the contribution of the forest floor efflux is larger than the contribution of the aboveground biomass to total ecosystem respiration. In the winter, modeled $\overline{F}(t, 0)$ can be as much as 85% of modeled R_E, while in the summer, it drops to about 70%. This finding is consistent with a recent study at the site based on stable isotope measurements and analysis [*Mortazavi et al.*, 2005].

4.5. CSO_E Model Testing

[40] To check the performance of the CSO_E model, we compare the monthly modeled forest floor carbon efflux with monthly $\overline{F}(t, 0)$ determined from chambers [*Palmroth et al.*,

2005] (Figure 6). When comparing the monthly data, the largest divergence between the chamber estimates and the CSO_E model is during the severe drought in 2002. It appears that the CSO_E model predictions of $\overline{F}(t, 0)$ are lower than estimates by the chambers suggesting oversensitivity to drought. Furthermore, the CSO_E model underpredicts the chamber-based high respiration rate. Despite these differences, there is a good agreement between these two independent estimates on annual timescales (Table 4). These differences result in CSO_E modeled efflux that is about 111 gC m^{-2} year^{-1} smaller than the chamber-based estimates. The difference might be attributed to several factors that are difficult to deconvolve: (1) The footprints of the chambers and CSO_E model are very different, and it is possible that the average of the patches sampled with the chambers consistently respired more than the area sampled by the mean concentration used in the CSO_E and (2) the CSO_E modeled turbulent diffusivity near the ground (highly sensitive to how $\overline{w'w'}$ and Q decay near the forest floor) may be consistently low (because of both model formulation of the mixing length and plant area distribution near the ground) thereby biasing the CSO_E model inversion to lower values.
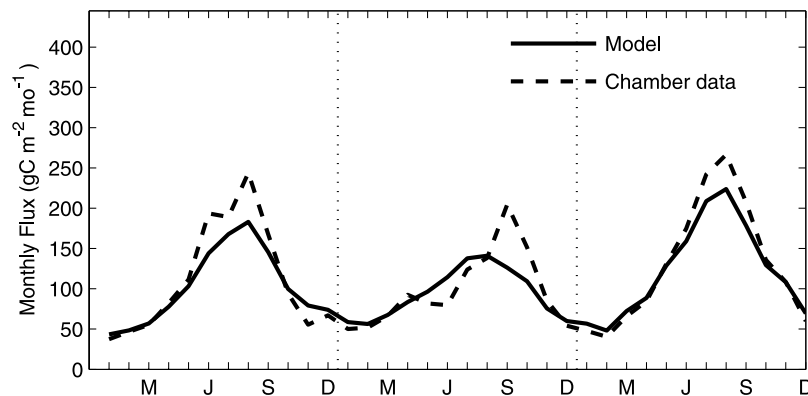

Figure 6. Comparisons between the monthly forest floor effluxes from CSO_E and the chamber data generated from the regression equation given by *Palmroth et al.* [2005] for all 3 years.

Table 4. Annual Carbon Budgets at the Duke Forest Pine Site From 2001 to 2003[a]

Carbon Budget Components	2001	2002	2003	Notes
Annual ecosystem respiration, R_E	1767	1623	2022	$R_E = F(t, 0) + R_{AB}$
Forest floor carbon efflux, $F(t, 0)$	1224	1127	1473	CSO_E model
	(1328)	(1230)	(1599)	ACES chamber exp.
	(1344)	(1180)	(1565)	ACES model equation (16)
Aboveground respiration, R_{AB}	543	498	549	CSO_E model = $\int_0^h S(t,z)dz$
(Dark respiration)	(391)	(387)	(412)	$\int_0^h [a(t,z) \cdot 0.015 \cdot V_{c\max}(t,z)]dz$
Total root respiration, R_R	673	620	810	$R_R = 0.55 \cdot F(t, 0)$[b]
Autotrophic respiration, R_A	1216	1118	1359	$R_A = R_R + R_{AB}$
Heterotrophic respiration, R_H	551	507	663	$R_H = 0.45 \cdot F(t, 0)$[b]
Modeled GPP	2211	2033	2471	$\frac{NPP}{GPP} = 1 - \left\|\frac{R_A}{GPP}\right\| \approx 0.45$[c]
Modeled NPP	995	915	1112	
Nighttime values				
R_E from CSO_E	837	791	987	
R_E from $F(t,h)$-PPFD curve	987	796	1033	
Fst	197	203	227	
F_{EC}	(616)	(691)	(759)	

[a]Unit is gC m^{-2} yr^{-1}.
[b]From *Andrews et al.* [1999].
[c]Estimated from data given by *Lai et al.* [2002b] and *Hamilton et al.* [2002].

Regardless of the reason, relative to the annual rate of forest floor efflux (>1000 gC m^{-2}), the difference in annual estimates based on these very different approaches is surprisingly small (about 10%), especially considering the large differences (23%) obtained using different approaches [*Law et al.*, 1999a].

[41] Finally, we compared $\overline{F_{EC}}$ with CSO_E modeled $\overline{F}(t,z)$ for different u^* thresholds and for the entire 3-year period (Figure 7). $\overline{F_{EC}}$ is consistently lower than modeled $\overline{F}(t,z)$ by almost 30% for small u^* and almost 8% for high u^*. Note that this comparison is a direct flux comparison between measured and modeled fluxes above the canopy and not a respiration comparison, which is dependent on storage flux estimates. To explore whether high-frequency corrections to $\overline{F_{EC}}$ (not applied to the EC data here) alone may explain this underestimation, we used the analytical model by *Massman* [2000]. For the model calculations (also shown as dashed line in Figure 7) we employed the following configuration: the CSAT3 sonic anemometer has collocated vertical and horizontal paths of length 0.15 m; the sampling period is 30 min; the sampling frequency is 10 Hz; the measurement height above the zero plane displacement is 9.95 m; no anti noise band pass filtering or detrending is used; block averaging is conducted every 30 min; planar separation distance between the CSAT3 and the LI7500 gas analyzer is 0.15 m with no vertical separation; and the LI7500 sensor path length is 0.20 m with a time constant determined by assuming line averaging only. The ensemble ratio of corrected to uncorrected fluxes predicted by this analytical model only explains about half of the differences of $\overline{F_{EC}}$ (i.e., 15%−4% with increasing u^*).

4.6. Nighttime Net Ecosystem Respiration Comparison: Effects of Atmospheric Stability

[42] In Figure 8, we compare the CSO_E model calculations assuming neutral atmospheric stability conditions with the density-stratified CSO_E model results for R_E. By setting $g = 0$ (i.e., the contribution from terms $\overline{T'C'}$ and $\overline{T'T'} = 0$) and not correcting the upper boundary conditions for atmospheric stability guarantee neutral stratification within the general CSO_E model. We found that by ignoring local atmospheric

stability, the modeled R_E is about 10% lower for the entire study period. For reference, Figure 9 also shows the nighttime ecosystem respiration comparison between the CSO_E model (solid lines) and $\overline{F_{EC}}$ (dot-dashed line) and $\overline{F_{EC}} + \overline{F_{st}}$ (dotted line). This comparison demonstrates that resolving the storage flux and correcting for local thermal stratification tends to increase R_E over its eddy covariance estimate (without storage). Interestingly, correcting for monthly storage fluxes may be comparable to correcting for the stability effects (∼20 gC m^{-2} month^{-1} in summer of 2003).

4.7. Ecosystem Carbon Budget at the Duke Forest Pine Site

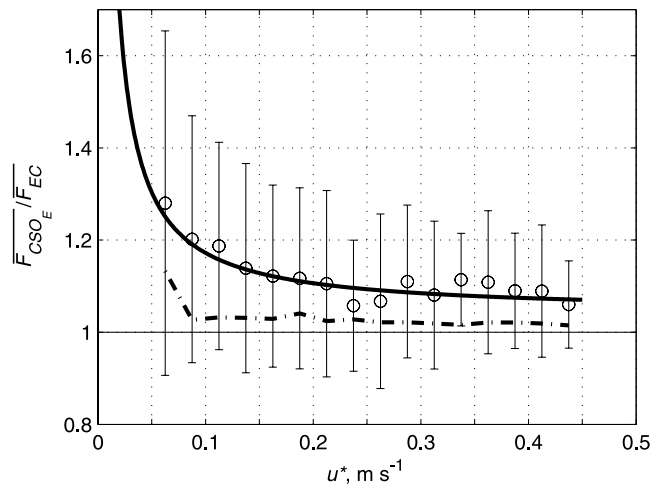[43] From the CSO_E model results, we summarize the carbon budget for the site from 2001 to 2003 (Table 4).

Figure 7. Ratio of modeled CSO_E flux above the canopy ($\overline{F_{CSO_E}}$) to that from eddy covariance measurements ($\overline{F_{EC}}$) in relation to the u_* threshold employed for data collected during the 3-year period. The circles are ensemble-averaged $\overline{F_{CSO_E}}/\overline{F_{EC}}$, and the vertical lines are one standard deviation around the average. The dot-dashed line is the high-frequency spectral corrections to the $\overline{F_{EC}}$ predicted by the *Massman* [2000] model.
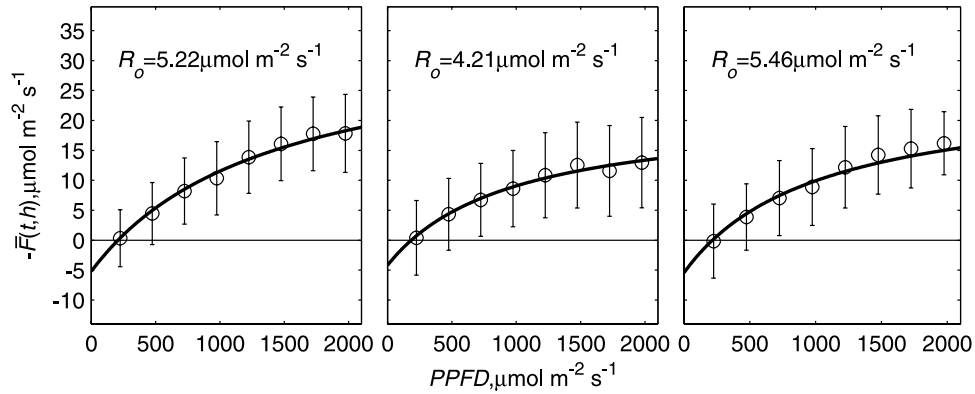
Figure 8. Canopy-scale light response curve determined from eddy covariance flux measurements and *PPFD* measurements at the top of canopy for each year. The open circle and error bar show the statistics (mean and standard deviation) of the flux measurement against different *PPFD* levels, and the solid line shows the fitted light response curve for each year. The values of R_o are shown for convenience.

Summing up the modeled forest floor carbon efflux and modeled aboveground respiration leads to total ecosystem respiration of 1767, 1623, and 2022 gC m^{-2}, respectively, for 2001, 2002, and 2003. These values are consistent with independent estimates made earlier at the site (see Table 4). To further assess whether the modeled R_E is also consistent with the expected overall carbon balance at the site, we estimated root respiration from $R_R = 0.55 \cdot \overline{F}(t, 0)$ [*Andrews et al.*, 1999] using CSO$_E$ modeled $\overline{F}(t, 0)$. The autotrophic respiration R_A can be determined from the R_R and the CSO$_E$ modeled aboveground respiration (R_{AB}). To determine gross primary production (GPP) and net primary production (NPP) from R_A, we used the following relationship:

$$\frac{NPP}{GPP} = 1 - \left| \frac{R_A}{GPP} \right|$$

Lai et al. [2002b] quantified the NPP/GPP ratio using aboveground biomass for a young (6 year old) pine stand. In this study, we used the averaged aboveground biomass of 5128 gC m^{-2} estimated by *Hamilton et al.* [2002] to determine the NPP/GPP ratio as about 0.45 for this study site. Using this estimate, the modeled GPP computed from modeled R_A varied from 2033 to 2471 gC m^{-2} for these 3 years. This range is comparable to other estimates

[*Hamilton et al.*, 2002; *Lai et al.*, 2002a; *Schafer et al.*, 2003] conducted earlier at the site (2371 to 2486 gC m^{-2} from 1998 to 2000). As for NPP, the modeled values here ranged from 915 to 1112 gC m^{-2} during the 3-year study period. This range is higher by about 200 gC m^{-2} when compared to biometric estimates [*Hamilton et al.*, 2002; *Schafer et al.*, 2003] conducted for an earlier period from 1998 to 2000 (705 to 1060 gC m^{-2}).

[44] Up to this point, we showed how the CSO$_E$ model is used to constrain annual nighttime respiration from CO_2 concentration data. Here, we compare these CSO$_E$ results to other proposed methods that attempt to constrain nighttime respiration. In particular, we used the so-called light response curve method [*Lee et al.*, 1999], which is based on determining the intercept of the $\overline{F}(t, h)$ and photosynthetically active photon flux density (*PPFD*) [*Clark et al.*, 1999; *Lai et al.*, 2002a; *Law et al.*, 1999a]. The curve is expressed as:

$$\overline{F}(t, h) = \frac{\omega_p \cdot PPFD \cdot F_{sat}}{\omega_p \cdot PPFD + F_{sat}} - R_o$$

where ω_p is the mean apparent quantum yield, F_{sat} is the net CO_2 flux at light saturation, and intercept R_o is the mean net CO_2 flux when *PPFD* = 0. The R_o can provide estimates of
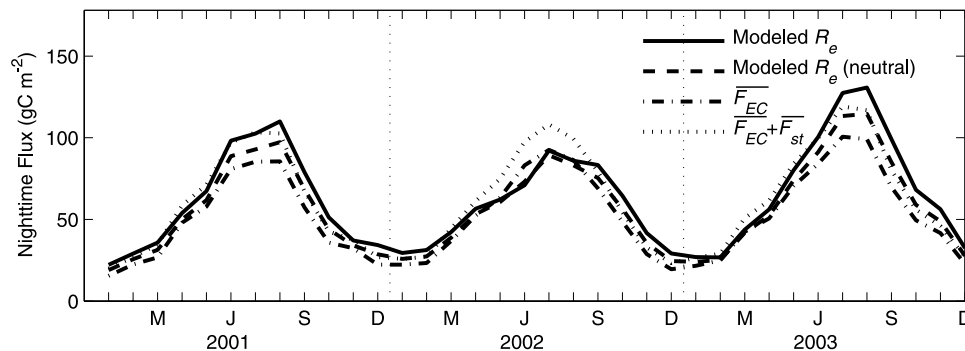

Figure 9. Comparison between nighttime (monthly ensemble average from 2000 to 0500 LT) ecosystem respirations obtained from eddy covariance measurements and CSO$_E$ model results with and without the consideration of atmospheric stability.

mean nighttime ecosystem respiration independent of the nocturnal CO_2 concentration or $\overline{F}(t, h)$ data.

[45] Figure 9 shows the light response curves for 2001 to 2003, respectively. The lower daytime fluxes in 2002 are due to the severe drought event. The R_o estimated for each year resulted in nighttime ecosystem respiration of 987, 796, and 1033 gC m^{-2} yr^{-1}, which are slightly higher than the estimates from the CSO_E model (higher by about 0.5% to 16%).

5. Conclusion

[46] We developed a Eulerian version of the constrained source optimization (CSO_E) model that considers local atmospheric stability and storage fluxes. The model uses simultaneous mean air temperature and mean CO_2 concentration profiles in the inversion for forest floor efflux and above ground source distribution. On the basis of model calculations and measurements at a maturing pine forest in the southeastern United States, we demonstrated the following:

[47] 1. At this study site, the contribution of the storage flux during nighttime conditions is at least 27% of the EC measured flux, even under high friction velocity $u*$ conditions.

[48] 2. Considering local atmospheric stability in the CSO_E model increases the modeled ecosystem annual respiration by about 10%, and can be comparable to storage fluxes.

[49] 3. The CSO_E model captures well forest floor carbon efflux during both wet and dry years. Also, the variation of the optimized aboveground source parameter is consistent with seasonal variation in $V_{cmax,25}$.

[50] 4. The CSO_E modeled CO_2 flux above the canopy was systematically higher than the eddy covariance measurements by about 30% for low $u*$ and about 10% for high $u*$. A separate analysis using the *Massman* [2000] analytical model revealed that high-frequency corrections to the eddy covariance measurements can explain only 50% of this difference.

[51] 5. The CSO_E modeled ecosystem respiration, when evaluated within the overall carbon balance at the site, appears consistent with various independent component estimates.

[52] 6. The CSO_E modeled ecosystem respiration agreed well with independent respiration estimates derived from the intercept of the annual $\overline{F}(t, h)$-*PPFD* light-response curves. This agreement lends support to a symbiotic use of both methods to further constrain nighttime ecosystem respiration.

[53] The broader implications of this work are twofold. Given the large uncertainties in R_E, a logical starting point is to derive multiple estimates of R_E, with each estimate sensitive to different assumptions. Chamber estimates provide bottom-up values with limited spatial extent; EC methods provide top-down estimates that can be linked to R_E using numerous assumptions and simplifications (but independent from the chamber data). Agreement between these estimates hints at a robust value for R_E, while disagreement flags uncertainties. The proposed CSO_E provides an additional, independent estimate of R_E at the EC spatial scale but has the decisive advantage over EC based

estimates because of its ability to separate forest floor effluxes from aboveground fluxes. Therefore the model can serve as a link between EC based measurements and chamber measurements of R_E, helping to isolate uncertainties in R_E originating from forest floor estimates from those generated by above ground estimates.

[54] The CSO_E model can be readily linked to stable isotope measurements. Information from stable isotope measurements can be combined into the CSO_E optimization by providing further constraints on the ratio of floor efflux and above ground CO_2 production at multiple levels within the canopy. The optimization solutions above ground can also be qualitatively assessed against expected shifts in physiological properties (e.g., $V_{cmax,25}$).

[55] Although the CSO_E model is a useful step for constraining nighttime R_E, certain difficulties remain. For example, the Eulerian formulation provided is one-dimensional and neglects topography-induced drainage flows. The closure formulations are derived assuming fully developed turbulence; an assumption that may frequently be violated at night. Last, the CSO_E formulation has several inconsistent "internal" approximations. For example, the assumption of nonsteady state means continuity equation (to account for mean storage fluxes) versus that of steady state flux budget equations (for simplicity).

Appendix A: Second-Order Closure Approximation

A1. Momentum and Reynolds Stress Budget Equations

[56] *Wilson and Shaw* [1977] proposed a set of higher-order closure approximations to parameterize each term in the momentum $\overline{u_i}$ equations, and utilized a method similar to *Mellor* [1973] for the closure the Reynolds stress $\overline{u_i' u_j'}$ equations. For higher-order closure approximation schemes, the gradient diffusion approximation introduced by *Mellor* [1973] and *Donaldson* [1973] is employed to close each term in the governing equations of fluxes.

[57] *Katul and Albertson* [1998] simplified *Wilson and Shaw* [1977] model by assuming horizontal homogeneity and steady state conditions and obtained the following closure approximation equations to describe the full budget of the longitudinal wind velocity component and corresponding Reynolds stresses.

$$\frac{\partial \overline{u}}{\partial t} = 0 = -C_d \cdot a \cdot \overline{u}^2 - \frac{\partial \overline{u'w'}}{\partial z} \qquad (A1a)$$

$$\frac{\partial \overline{u'w'}}{\partial t} = 0 = -\overline{w'w'}\frac{\partial \overline{u}}{\partial z} - \frac{Q\overline{u'w'}}{3\lambda_2} + C_w Q^2 \frac{\partial \overline{u}}{\partial z} - \frac{\partial \overline{w'u'w'}}{\partial z} \quad (A1b)$$

$$\frac{\partial \overline{u'u'}}{\partial t} = 0 = -2\left(\overline{u'w'}\frac{\partial \overline{u}}{\partial z} + \overline{u}\frac{\partial \overline{u'w'}}{\partial z}\right) - \frac{Q}{3\lambda_1}\left(\overline{u'u'} - \frac{Q^2}{3}\right) - \frac{2}{3}\frac{Q^3}{\lambda_3} - \frac{\partial \overline{w'u'u'}}{\partial z} \qquad (A1c)$$

$$\frac{\partial \overline{v'v'}}{\partial t} = 0 = -\frac{Q}{3\lambda_1}\left(\overline{v'v'} - \frac{Q^2}{3}\right) - \frac{2}{3}\frac{Q^3}{\lambda_3} - \frac{\partial \overline{w'v'v'}}{\partial z} \qquad (A1d)$$
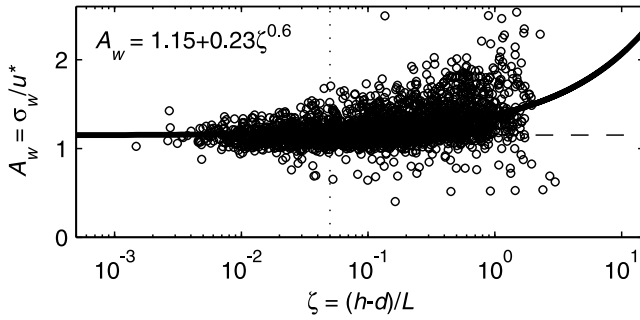
Figure A1. Relationship between A_w and atmospheric stability parameter ζ. All the data points are from EC measurements above the canopy from 2001 to 2003. Neutral atmospheric stability conditions are defined when the absolute value of ζ is less than 0.05 (the dotted vertical line) [*Siqueira and Katul*, 2002]. The dashed line represents the mean value (1.15) of A_w under neutral atmospheric stability, and the solid line is the fitted curve.

$$\frac{\partial \overline{w'w'}}{\partial t} = 0 = -\frac{Q}{3\lambda_2}\left(\overline{w'w'} - \frac{Q^2}{3}\right) - \frac{2}{3}\frac{Q^3}{\lambda_3} + \frac{2g}{\overline{T}}\overline{w'T'} - \frac{\partial \overline{w'w'w'}}{\partial z}$$

(A1e)

where Q is the characteristic turbulent velocity (square root of the mean turbulent kinetic energy $\sqrt{\overline{u_i'u_i'}}$), and C_d is the drag coefficient. Parameters λ_1, λ_2, and λ_3 are the characteristic length scales as discussed in section 2.1. These three length scales are determined from the mixing length, $L(z)$ ($\lambda_i = a_i \times L$, where $i = 1, 2, 3$), where a_i and C_w are the constants to be determined in Appendix A.2.

[58] In equations (A1a), the closure approximations of all the triple correlation terms are described in Appendix A.3.

A2. Determination of Closure Constants and the Stability Dependency

[59] Applying the linear relationship between σ_{ui} and $u*$ above the canopy in the neutral surface layer results in:

$$\sigma_u = A_u \cdot u*$$
$$\sigma_v = A_v \cdot u*$$ (A2)
$$\sigma_w = A_w \cdot u*$$

$$Q = \sqrt{A_1^2 + A_v^2 + A_w^2} \cdot u* = A_Q \cdot u*$$

where A_u, A_v, and A_w could be obtained from the eddy covariance measurement [*Katul and Albertson*, 1998; *Shaw*, 1977].

[60] To derive the relationship between A_w and atmospheric stability, we used the EC data from 2001 to 2003 and plotted A_w against the stability ($\zeta = \frac{(h-d)}{L}$, where d is the zero-plane displacement derived from $\overline{u'w'}$ profiles [*Katul and Albertson*, 1998]), as shown in Figure A1. The fitted curve is

$$A_w = 1.15 + 0.23 \cdot \zeta^{0.6}$$ (A3a)

and is employed to quantify A_w for different atmospheric stability conditions. The number 1.15 in equation (A3a) is

the mean value of A_w at neutral stability. The variations of A_u and A_v for different stability conditions were obtained using the same procedure:

$$A_u = 1.96 + 0.49 \cdot \zeta^{0.5}$$ (A3b)

$$A_v = 1.94 + 0.47 \cdot \zeta^{0.5}$$ (A3c)

[61] The corresponding value of A_Q then can be derived from A_u, A_v and A_w.

[62] To quantify the effect of canopy structure and atmospheric stability on the momentum component profiles, we present the vertical distributions of modeled $\sigma_w/u*$ and $Q/u*$ for two distinct plant area density distributions and for both neutral ($|\zeta| \leq 0.05$) and stable ($\zeta = 1.2$) stability conditions in Figure A2. From Figure A2, we found that atmospheric stability is much more important than the variations of PAD.

[63] By using the parameters derived above, *Katul and Albertson* [1998] summarize the following equations,

$$a_2^{-1}\left(A_w^2 - \frac{A_Q^2}{3}\right) + a_3^{-1}\left(2A_Q^2\right) + C(0) = 0$$

$$a_2^{-1}\left(A_u^2 - \frac{A_Q^2}{3}\right) + a_3^{-1}\left(2A_Q^2\right) + C(0) = \frac{6}{A_Q}$$ (A4)

$$a_2^{-1}\left(\frac{1}{3A_Q^2}\right) + a_3^{-1}(0) + C(1) = \left(\frac{A_w}{A_Q}\right)^2$$

to determine the value of closure constant a_2, a_3 and C_w. The value of a_1 is determined by the equation $a_1 = \frac{1}{A_Q}$ [*Katul and Albertson*, 1998; *Shaw et al.*, 1974]

A3. Second-Order Closure Parameterization for Triple Correlations

[64] For the triple velocity correlation components, the general form of the second-order closure model param-
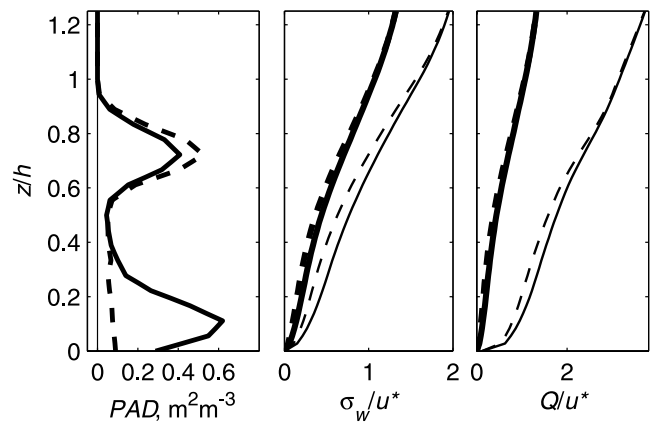

Figure A2. Sensitivity of plant area density (PAD) and atmospheric stability to closure model predictions. (left) Two end-members of the measured PAD profiles (solid line for day 124 and dashed line for day 329). The bold lines and thin lines represent neutral ($|\zeta| \leq 0.05$) and stable ($\zeta = 1.2$) atmospheric stability conditions, respectively, for (middle) $\sigma_w/u*$ and (right) $Q/u*$. The solid lines and dashed lines in the middle and right plots correspond to the PAD profiles shown in the left plot.

eterizations are [*Katul and Albertson*, 1998; *Mellor*, 1973]:

$$\overline{u_i' u_j' u_k'} = -Q\lambda_1 \left(\frac{\partial \overline{u_i' u_j'}}{\partial x_k} + \frac{\partial \overline{u_j' u_k'}}{\partial x_i} + \frac{\partial \overline{u_k' u_i'}}{\partial x_j} \right) \qquad (A5)$$

[65] The one-dimensional closure approximation for the transport of scalar fluxes and buoyant terms can be express as follows:

$$\overline{w' w' C'} = -Q\lambda_1 \left(\frac{\partial \overline{F}}{\partial z} \right)$$

$$\overline{w' w' T'} = -Q\lambda_1 \left(\frac{\partial \overline{F_T}}{\partial z} \right) \qquad (A6)$$

and

$$\overline{w' T' C'} = -Q\lambda_1 \left(\frac{\partial \overline{T' C'}}{\partial z} \right)$$

$$\overline{w' T' T'} = -Q\lambda_1 \left(\frac{\partial \overline{T' T'}}{\partial z} \right) \qquad (A7)$$

Appendix B: Theoretical and Practical Issues for Estimating Storage Flux at a Single Tower

[66] The $u*$ thresholds are often employed for multiple reasons:

[67] 1. The first reason is to eliminate nonturbulent conditions. For example, *Cava et al.* [2004] showed how canopy waves are generated and how they can transport significant CO_2 inside to outside and outside to inside the canopy and over periods that if not properly captured by the averaging interval can lead to negative CO_2 fluxes (i.e., photosynthesis like) at night. Employing a $u*$ threshold is primarily to ensure that runs collected under such nonturbulent conditions are removed.

[68] 2. The second reason is to reduce high-frequency losses. Eddy covariance fluxes themselves suffer from high-frequency cospectral losses under moderately stable and very stable atmospheric conditions due to instrument separation distances, limited sampling frequency, and path length averaging by instruments. So, filtering by $u*$ eliminates those runs. There are ways to correct for some of those losses using temperature time series data, but the similarity between CO_2 and temperature breaks down even at high frequency for very stable conditions [see *Katul and Parlange*, 1994].

[69] 3. The third reason is to minimize the effect of storage flux on the estimate of ecosystem respiration from eddy covariance data. The difficulty in estimating the storage flux that is most consistent with the scalar continuity equation can be demonstrated as follows: the depth-integrated 1-D continuity equation:

$$\int_0^h \frac{\partial \overline{C}}{\partial t} dz = -F(h) + \left[F(0) + \int_0^h \overline{S} dz \right]$$

and this equation is a spatially averaged equation. The term in parentheses is the desired ecosystem respiration (R_E) (spatially averaged). The origin of the term $\int_0^h S dz$ arises because of spatially averaging (after temporally averaging

say over half an hour) the point equations. Now, to correctly estimate the spatially averaged R_E, one must determine the spatially averaged $\int_0^h \frac{\partial \overline{C}}{\partial t} dz$. Estimating this quantity from a single tower at half hourly time step assumes that we have sampled all the volume within the averaging domain numerous times (to ensure sufficient sample size for the purposes of statistical averaging stability). For low winds inside the canopy, this convergence is problematic. For stronger winds (or higher $u*$ above the canopy), one is likely to sample, at the tower, fluid parcels originating from further distances, thereby ensuring that a bigger volume has been sampled over a 30 min period at a given point. This is primarily the ergodic hypothesis (in space), likely to be more accurate at higher $u*$ than lower $u*$. Alternatively, one can construct an ensemble of $\int_0^h \frac{\partial \overline{C}}{\partial t} dz$ for similar $u*$ and temperature and average those ensemble values assuming that the ensemble average better represents the spatial at the tower when compared to an individual half hour run. In all cases, a major uncertainty remains in the determination of $\int_0^h \frac{\partial \overline{C}}{\partial t} dz$ from a single tower, exasperated by low $u*$ conditions. This was the main reason for choosing a 14-day ensemble average: to ensure that the spatial average is estimated from ensemble averages rather than half hour rums. The 14-day period was chosen because the respiring biomass did not drastically change. There is another practical advantage to using ensemble averages vis à vis single runs, which is a reduction in the random error known to contaminate CO_2 concentration samples.

References

Andrews, J. A., K. G. Harrison, R. Matemala, and W. H. Schlesinger (1999), Separation of root respiration from total soil respiration using ^{13}C labeling during Free-Air-CO_2 Enrichment (FACE), *Soil Sci. Soc. Am. J.*, *63*, 1429–1435.

Baldocchi, D. D., R. Valentini, S. Running, W. Oechel, and R. Dahlman (1996), Strategies for measuring and modelling carbon dioxide and water vapour fluxes over terrestrial ecosystems, *Global Change Biol.*, *2*, 159–168.

Baldocchi, D. D., et al. (2001), FLUXNET: A new tool to study the temporal and spatial variability of ecosystem-scale carbon dioxide, water vapor and energy flux densities, *Bull. Am. Meteorol. Soc.*, *82*, 2415–2435.

Butnor, J. R., and K. H. Johnsen (2004), Calibrating soil respiration measures with a dynamic flux apparatus using artificial soil media of varying porosity, *Eur. J. Soil Sci.*, *55*, 639–647.

Butnor, J. R., K. H. Johnsen, and R. Oren (2003), Reduction of forest floor respiration by fertilization on both carbon dioxide-enriched and reference 17-year-old loblolly pine stands, *Global Change Biol.*, *9*, 849–861.

Campbell, G. S., and J. M. Norman (1998), Plants and plant communities, in *An Introduction to Environmental Biophysics*, pp. 223–246, Springer, New York.

Cava, D., U. Giostra, M. Siqueira, and G. G. Katul (2004), Organized motion and radiative perturbations in the nocturnal canopy sublayer above an even-aged pine forest, *Boundary Layer Meteorol.*, *112*, 129–157.

Clark, K. L., H. L. Gholz, J. B. Moncrieff, F. Cropley, and H. W. Loescher (1999), Environmental controls over net exchanges of carbon dioxide from contrasting Florida ecosystems, *Ecol. Appl.*, *9*, 936–948.

Collatz, G. J., T. Ball, C. Crivet, and J. A. Berry (1991), Physiological and environmental regulation of stomatal conductance, photosynthesis and transpiration: A model that includes a laminar boundary layer, *Agric. For. Meteorol.*, 54, 107–136.

Corrsin, S. (1974), Limitations of gradient transport models in random walks and in turbulence, *Adv. Geophys.*, 18A, 25–60.

Deardorff, J. W. (1972), Numerical investigation of neutral and unstable planetary boundary layers, *J. Atmos. Sci.*, 29, 91–115.

Deardorff, J. W. (1978), Closure of second and third moment rate equations for diffusion in homogeneous turbulence, *Phys. Fluids*, 21, 525–530.

De Bruin, H. A. R., W. Kohsiek, and B. J. J. M. van den Hurk (1993), A verification of some methods to determine the fluxes of momentum, sensible heat, and water vapor using standard deviation and structure parameter of scalar meteorological quantities, *Boundary Layer Meteorol.*, 63, 231–257.

Denmead, O. T., and E. F. Bradley (1985), Flux-gradient relationships in a forest canopy, in *The Forest-Atmosphere Interaction*, edited by B. A. Hutchison and B. B. Hicks, pp. 421–442, Springer, New York.

Donaldson, C. D. (1973), Construction of a dynamic model of the production of atmospheric turbulence and the dispersal of atmospheric pollutants, paper presented at Workshop on Micrometeorology, Am. Meteorol. Soc., Boston, Mass.

Ellsworth, D. S. (1999), CO_2 Enrichment in a maturing pine forest: Are CO_2 exchange and water status in the canopy affected?, *Plant Cell Environ.*, 22, 461–472.

Ellsworth, D. S. (2000), Seasonal CO_2 assimilation and stomatal limitations in a Pinus taeda canopy, *Tree Physiol.*, 20, 435–445.

Fang, C., and J. B. Moncrieff (1999), A model for soil CO_2 production and transport 1: Model development, *Agric. For. Meteorol.*, 95, 225–236.

Farquhar, G. D., S. Von Caemmerer, and J. A. Berry (1980), A biochemical model of photosynthetic CO_2 assimilation in leaves of C_3 species, *Planta*, 149, 79–90.

Finnigan, J. J. (1985), Turbulent transport in plant canopies, in *The Forest-Atmosphere Interaction*, edited by B. A. Hutchison and B. B. Hicks, pp. 443–480, Springer, New York.

Goulden, M. L., J. W. Munger, S.-M. Fan, B. C. Daube, and S. C. Wofsy (1996), Exchange of carbon dioxide by a deciduous forest: Response to interannual climate variability, *Science*, 271, 1576–1578.

Hamilton, J. G., E. H. DeLucia, K. George, S. L. Naidu, A. C. Finzi, and W. H. Schlesinger (2002), Forest carbon balance under elevated CO_2, *Oecologia*, 131, 250–260.

Hsieh, C. I., M. Siqueira, G. G. Katul, and C. R. Chu (2003), Predicting scalar source-sink and flux distribution withins within a forest canopy using 2-D Lagrangian stochastic model, *Boundary Layer Meteorol.*, 109, 113–138.

Kaimal, J. C., and J. J. Finnigan (1994), Flow over plant canopies, in *Atmospheric Boundary Layer Flows: Their Structure and Measurements*, pp. 66–108, Oxford Univ. Press, New York.

Kaimal, J. C., and J. E. Gaynor (1991), Another look at sonic thermometry, *Boundary Layer Meteorol.*, 56, 401–410.

Katul, G. G., and J. D. Albertson (1998), An investigation of higher-order closure model for a forested canopy, *Boundary Layer Meteorol.*, 89, 47–74.

Katul, G. G., and J. D. Albertson (1999), Modeling CO_2 sources, sinks, and fluxes within a forest canopy, *J. Geophys. Res.*, 104, 6081–6091.

Katul, G. G., and M. B. Parlange (1994), On the active role of temperature in surface layer turbulence, *J. Atmos. Sci.*, 51, 2181–2195.

Katul, G. G., D. Ellsworth, and C.-T. Lai (2000), Modeling assimilation and intercellular CO2 from measured conductance: A synthesis of approaches, *Plant Cell Environ.*, 23, 1313–1328.

Katul, G. G., L. Mahrt, D. Poggi, and C. Sanz (2004), One and two equation models for canopy turbulence, *Boundary Layer Meteorol.*, 113, 91–109.

Lai, C.-T., G. G. Katul, D. Ellsworth, and R. Oren (2000a), Modelling vegetation-atmosphere CO_2 exchange by a coupled Eulerian-Lagrangian approach, *Boundary Layer Meteorol.*, 95, 91–122.

Lai, C.-T., G. G. Katul, R. Oren, D. Ellsworth, and K. Schafer (2000b), Modeling CO_2 and water vapor turbulent flux distributions within a forest canopy, *J. Geophys. Res.*, 105, 26,333–26,351.

Lai, C.-T., G. G. Katul, J. Butnor, D. Ellsworth, and R. Oren (2002a), Modelling night-time ecosystem respiration by a constrained source optimization method, *Global Change Biol.*, 8, 124–141.

Lai, C.-T., G. G. Katul, J. R. Butnor, M. Siqueira, D. S. Ellsworth, C. Maier, K. H. Johnsen, S. McKeand, and R. Oren (2002b), Modeling the limits on the response of net carbon exchange to fertilization in a southeastern pine forest, *Plant Cell Environ.*, 25, 1095–1119.

Law, B. E., D. D. Baldocchi, and P. M. Anthoni (1999a), Below-canopy and soil CO_2 fluxes in a ponderosa pine forest, *Agric. For. Meteorol.*, 94, 171–188.

Law, B. E., M. G. Ryan, and P. M. Anthoni (1999b), Seasonal and annual respiration of a ponderosa pine ecosystem, *Global Change Biol.*, 5, 169–182.

Lee, X. H., J. D. Fuentes, R. M. Staebler, and H. H. Neumann (1999), Long-term observation of the atmospheric exchange of CO_2 with a temperate deciduous forest in southern Ontario, Canada, *J. Geophys. Res.*, 104, 15,975–15,984.

Leuning, R. (2000), Estimation of scalar sources/sink distributions in plant canopies using Lagrangian dispersion analysis: Corrections for atmospheric stability and comparison with a multilayer canopy model, *Boundary Layer Meteorol.*, 96, 293–314.

Leuning, R., and M. J. Judd (1996), The propagation of errors in long term measurements of land atmosphere fluxes of carbon and water, *Global Change Biol.*, 2, 231–240.

Lindroth, A., A. Grelle, and A.-S. Morén (1998), Long-term measurements of boreal forest carbon balance reveal large temperature sensitivity, *Global Change Biol.*, 4, 443–450.

Massman, W. J. (2000), A simple method for estimating frequency response corrections for eddy covariance systems, *Agric. For. Meteorol.*, 104, 185–198.

Mellor, G. (1973), Analytic prediction of the properties of stratified planetary boundary layer, *J. Atmos. Sci.*, 30, 1061–1069.

Mellor, G., and T. Yamada (1974), A hierarchy of turbulence closure models for plenstary boundary layers, *J. Atmos. Sci.*, 31, 1791–1806.

Meyers, T., and K. T. Paw U (1986), Testing of a higher-order closure model for modeling airflow within and above plant canopies, *Boundary Layer Meteorol.*, 37, 297–311.

Meyers, T., and K. T. Paw U (1987), Modeling the plant canopy micrometeorology with higher-order closure principles, *Agric. For. Meteorol.*, 41, 143–163.

Moncrieff, J. B., Y. Malhi, and R. Leuning (1996), The propagation of errors in long-term measurements of land atmosphere fluxes of carbon and water, *Global Change Biol.*, 2, 231–240.

Mortazavi, B., J. P. Chanton, J. L. Prater, A. C. Oishi, R. Oren, and G. G. Katul (2005), Temporal variability in ^{13}C of respired CO_2 in a pine and a hardwood forest subject to similar climatic conditions, *Oecologia*, 142, 57–69.

Naumburg, E., and D. S. Ellsworth (2000), Photosynthetic sunfleck utilization potential of understory saplings growing under elevated CO_2 in FACE, *Oecologia*, 122, 163–174.

Naumburg, E., D. S. Ellsworth, and G. G. Katul (2001), Modeling daily understory photosynthesis of species with differing photosynthetic light dynamics in ambient and elevated CO_2, *Oecologia*, 126, 487–499.

Palmroth, S., C. A. Maier, H. R. McCarthy, A. C. Oishi, H.-S. Kim, K. H. Johnsen, G. G. Katul, and R. Oren (2005), Contrasting responses to drought of forest floor CO_2 efflux in a Loblolly pine plantation and a nearby oak-hickory forest, *Global Change Biol.*, 11, 1–14.

Pataki, D. E., R. Oren, and D. T. Tissue (1998), Elevated carbon dioxide does not affect average canopy stomatal conductance of Pinus taeda L., *Oecologia*, 117, 47–52.

Raupach, M. R. (1988), Canopy transport processes, in *Flow and Transport in the Natural Environment: Advances and Applications*, edited by W. L. Steffen and O. T. Denmead, pp. 95–127, Springer, New York.

Raupach, M. R. (1989a), Applying Lagrangian fluid mechanics to infer scalar source distributions from concentration profiles in plant canopies, *Agric. For. Meteorol.*, 47, 85–108.

Raupach, M. R. (1989b), A practical Lagrangian method for relating scalar concentrations to source distributions in vegetation canopies, *Q. J. R. Meteorol. Soc.*, 115, 609–632.

Schafer, K. V. R., R. Oren, D. S. Ellsworth, C.-T. Lai, J. D. Herrick, A. C. Finzi, D. D. Richter, and G. G. Katul (2003), Exposure to an enriched CO_2 atmosphere alters carbon assimilation and allocation in a pine forest ecosystem, *Global Change Biol.*, 9, 1378–1400.

Schmid, H.-P., C. Susan, B. Grimmond, F. Cropley, B. Offerle, and H.-B. Su (2000), Measurements of CO_2 and energy fluxes over a mixed hardwood forest in the mid-western United States, *Agric. For. Meteorol.*, 103, 357–374.

Shaw, R. H. (1977), Secondary wind speed maxima inside plant canopies, *J. Appl. Meteorol.*, 16, 514–521.

Shaw, R. H., G. den Hartog, K. M. King, and G. W. Thurtell (1974), Measurements of mean wind flow and three-dimensional turbulence intensity within a mature corn canopy, *Agric. For. Meteorol.*, 13, 419–425.

Siqueira, M., and G. Katul (2002), Estimating heat sources and fluxes in thermally stratified canopy flows using higher-order closure models, *Boundary Layer Meteorol.*, 103, 125–142.

Siqueira, M., G. Kutal, and C.-T. Lai (2002), Quantifying net ecosystem exchange by multilevel ecophysiological and turbulent transport models, *Adv. Water Resour.*, 25, 1357–1366.

Siqueira, M., R. Leuning, O. Kolle, F. M. Kelliher, and G. G. Katul (2003), Modeling sources and sinks of CO_2, H_2O and heat within a Siberian

pine forest using three inverse methods, *Q. J. R. Meteorol. Soc.*, *129*, 1373–1393.

Sreenivasan, K. R., S. Tavoularis, and S. Corrsin (1982), A test of gradient transport and its generalization, in *Turbulent Shear Flow III*, pp. 96–112, Springer, New York.

Styles, J. M., et al. (2002), Soil and canopy CO_2, $^{13}CO_2$, H_2O and sensible heat flux partitions in a forest canopy inferred from concentration measurements, *Tellus, Ser. B*, *54*, 655–676.

Valentini, R., et al. (2000), Respiration as the main determinant of carbon balance in European forests, *Nature*, *404*, 861–865.

Webb, E. K., G. I. Pearman, and R. Leuning (1980), Correction of flux measurements for density effects due to heat and water vapour transfer, *Q. J. R. Meteorol. Soc.*, *106*, 85–100.

Wilson, J. D. (1989), Turbulent transport within the plant canopy, in *Estimation of Areal Evapotranspiration*, pp. 43–80, IAHS Publ., Gentbrugge, Belgium.

Wilson, N. R., and R. H. Shaw (1977), A higher order closure model for canopy flow, *J. Appl. Meteorol.*, *16*, 1198–1205.

Wofsy, S. C., M. L. Goulden, J. W. Munger, S.-M. Fan, P. S. Bakwin, B. C. Daube, S. L. Bassow, and F. A. Bazzaz (1993), Net exchange of CO_2 in a mid-latitude forest., *Science*, *260*, 1314–1317.

Woodwell, G. M., and W. R. Dykeman (1966), Respiration of a forest measured by carbon dioxide accumulation during temperature inversions, *Science*, *154*, 1031–1034.

―――――――――――

J.-Y. Juang, G. G. Katul, H.-S. Kim, H. R. McCarthy, R. Oren, S. Palmroth, M. B. S. Siqueira, and P. C. Stoy, Nicholas School of the Environment and Earth Sciences, Duke University, Box 90328, Durham, NC 27708-0328, USA. (jj19@duke.edu)